

# Recent advancements of wide-angle polarization analysis with $^3\text{He}$ neutron spin filters

W.C. Chen<sup>1,2</sup>, T.R. Gentile<sup>1</sup>, Q. Ye<sup>1,2</sup>, A. Kirchhoff<sup>1</sup>, S.M. Watson<sup>1</sup>,  
J.A. Rodriguez-Rivera<sup>1,2</sup>, Y. Qiu<sup>1</sup>, C. Broholm<sup>1,3</sup>

<sup>1</sup> National Institute of Standards and Technology, Gaithersburg, Maryland 20899, USA

<sup>2</sup> University of Maryland, College Park, Maryland 20742, USA

<sup>3</sup> John Hopkins University, Baltimore, Maryland 21218, USA

E-mail: [wcchen@nist.gov](mailto:wcchen@nist.gov)

## Abstract.

Wide-angle polarization analysis with polarized  $^3\text{He}$  based neutron spin filters (NSFs) has recently been employed on the Multi-Axis Crystal Spectrometer (MACS) at the National Institute of Standards and Technology Center for Neutron Research (NCNR). Over the past several years, the apparatus has undergone many upgrades to address the fundamental requirements for wide angle polarization analysis using spin exchange optical pumping based  $^3\text{He}$  NSFs. In this paper, we report substantial improvements in the on-beam-line performance of the apparatus and progress toward routine user capability. We discuss new standard samples used for  $^3\text{He}$  NSF characterization and the flipping ratio measurement on MACS. We further discuss the management of stray magnetic fields produced by operation of superconducting magnets on the MACS instrument, which can significantly reduce the  $^3\text{He}$  polarization relaxation time. Finally, we present the results of recent development of horseshoe-shaped wide angle cells.

Key words: wide angle polarization analysis, wide angle  $^3\text{He}$  cell, horseshoe-shaped  $^3\text{He}$  cell, polarized  $^3\text{He}$  SEOP,  $^3\text{He}$  NSF

## 1. Introduction

Polarized neutron scattering is one of the most challenging neutron instrumentation techniques due to significant intensity reduction from polarized beam production and analysis, necessity of precise spin manipulation, and complicated data reduction and analysis. Supermirrors and Heusler crystals have been successfully employed to polarize the incident beam and analyze the scattered beam for decades. Recently, many modern neutron instrumentation techniques call for larger beam angular divergences and wavelength bandwidths, and a larger area of detector banks in the interest of large on-sample neutron fluxes and improved detection efficiency. This has made it difficult to apply the standard neutron polarization techniques using supermirrors or Heusler crystals.  $^3\text{He}$  neutron spin filters (NSF) are advantageous in (1) polarizing a broad wavelength band of neutrons effectively; (2) polarizing large area and widely divergent neutron beams; and (3) efficiently flipping the neutron polarization by reversing the  $^3\text{He}$  nuclear polarization using the adiabatic fast passage (AFP) nuclear magnetic resonance (NMR) technique[1]. The development of  $^3\text{He}$  NSFs has been advanced significantly during the last decade and these NSF devices have been applied or planned to be applied to many polarized neutron instrumentation



techniques in most neutron facilities worldwide[2, 3, 4, 5, 6, 7]. Recently, there has been much increased interest in wide angle polarization analysis using  $^3\text{He}$  NSF[6, 8, 9, 10, 11, 12].

The Multi-Axis Crystal Spectrometer (MACS)[13] at the National Institute of Standards and Technology (NIST) Center for Neutron Research (NCNR) is one of such modernized spectrometers where polarized beam instrumentation cannot be implemented with conventional neutron polarizing devices. Two existing and operating instruments with wide angle polarization analysis, D7[14] at the Institut Laue-Langevin and DNS[15] at the Jülich Centre for Neutron Science (JCNS), have employed supermirrors with a total cross sectional area of several hundred of square meters as the wide angle spin analyzer. A  $^3\text{He}$  NSF-based wide angle polarization analysis apparatus has recently been developed on MACS[10, 11]. Combined with high incident beam flux and multi-detector banks, MACS provides an improvement in polarized neutron detection efficiency by at least two orders of magnitude compared to the conventional cold triple-axis spectrometer SPINS at the NCNR. Very recently, we have primarily focused on improving the on-beam-line performance of the apparatus for routine user experiments. We describe substantial improvements of the wide angle polarization analysis capability, including standard samples for  $^3\text{He}$  NSF characterization, reduced magnetic field gradients, and fabrication of horseshoe cells. These advancements, combined with experience from several user experiments done recently, will make routine polarized MACS capability available soon.

## 2. Description of wide angle polarization analysis setup on MACS

MACS has recently been moved to the BT-9 beam line at the NCNR with a dedicated cold hydrogen source, and is operational now for routine user experiments[13]. MACS covers an incident energy range from 2.3 meV to 17 meV and typical final energies between 2.5 meV and 5 meV. MACS has a 34 cm by 42 cm monochromator consisting of 357 Pyrolytic Graphite (PG) crystals. This allows for doubly focusing the incident beam at the sample, providing an incident neutron beam flux up to  $5 \times 10^8 \text{ cm}^{-2}\text{s}^{-1}$ [13]. The detector system on MACS consists of 20 detector banks, each separated by  $8^\circ$ . Each detector channel has a conventional  $90^\circ$  Söller collimator. The scattering angle coverage depends on the incident energy and is different between negative and positive sides of the scattering angle. Following the neutron beam trajectory, positive scattering angles are located on the right side of the beam and negative scattering angles are located on the left side of the beam. The scattering angle reaches the maximum, about  $128^\circ$  on the negative scattering angle side at the highest incident energy and about  $115^\circ$  on the positive scattering angle side at the lowest incident energy. MACS allows for high sensitivity to access physics in small samples and is ideal for probing slowly propagating excitations in hard condensed matter.

Wide-angle polarization analysis on MACS has been developed using  $^3\text{He}$  NSFs and such an apparatus on MACS has been described in detail in previous papers[10, 11]. Here we outline the polarized beam setup. The polarized beam apparatus consists of a cylindrical  $^3\text{He}$  spin filter cell in a radio frequency(RF)-shielded square solenoid to polarize the incident neutron beam and two three-sectioned wide-angle  $^3\text{He}$  cells located near the sample and on opposite sides of the main beam to spin-analyze the scattered beam. Both the cells and the sample are contained within a uniform magnetic field of less than 4 mT provided by a vertical, neutron compatible solenoid. Therefore, the wide angle polarization analysis capability on MACS refers to uniaxial polarization analysis with the neutron polarization axis perpendicular to the scattering vector. Neutron spin flipping of the polarized beam is accomplished by inverting the  $^3\text{He}$  polarization using the AFP NMR technique. When flipping the neutron spin of the polarizer, the polarization loss to the analyzer is ensured to be negligible. The loss for the polarizer was 0.10 % per flip and the associated loss in the analyzer cell was 0.005 % per flip[11]. During the experiment, FID is used to monitor the  $^3\text{He}$  polarization in the spin filter cells. The  $^3\text{He}$  gas is polarized in sealed cells off the neutron beam line by spin-exchange optical pumping (SEOP) and the cells are

transported to the beam line in a portable solenoid. Recently, we reported several upgrades to this apparatus[11], in particular the development of GE180[16] wide-angle cells with relaxation times between 100 h and 400 h, and  $^3\text{He}$  polarization values,  $P_{\text{He}}$ , between 0.65 and 0.80. Using conventional cylindrical cells with a small angular coverage[17], the apparatus was employed for a study of superconducting  $\text{Fe}_{1+y}\text{Te}_{0.62}\text{Se}_{0.38}$ [18]. After substantial improvements of polarized MACS capability reported in reference[11] and discussed in this paper, several user experiments involving wide angle polarization analysis have been successfully completed and data analysis is in progress.

### 3. Standardized samples for $^3\text{He}$ NSF characterization

A sapphire powder sample was used at the very beginning of the polarized MACS development. Sapphire powder has several Bragg peaks. However, only the (012) peak with a d-spacing of 3.482 Å can be observed for both positive and negative scattering angles on the MACS instrument at 5 meV. One of the disadvantages of the sapphire sample is that the Bragg peak intensity is not very strong, requiring a fully open incident beam for quick and accurate measurements of the  $^3\text{He}$  polarization. This makes it inconvenient to perform transmission measurements of a  $^3\text{He}$  NSF[19] for a routine user experiment. Peak scans on a strong nuclear Bragg peak are typically used for transmission measurements so that the background from the sample and the  $^3\text{He}$  cell glass material can be removed. In order to observe Bragg peaks on both sides of the neutron beam at energies less than 5 meV, a large d-spacing crystal is necessary. Naturally occurring materials with a d-spacing on the order of 7-10 Å are not generally available. We are aware of two synthetic materials, mica[20] and intercalated graphite[21]. We chose to employ mica due to availability at the NCNR. The lattice spacing of the synthetic mica, fluorophlogopite, has been measured to be  $d = 9.963$  Å. So the scattering angles  $2\theta$  are 33.4 °, 27.3 °, and 23.4 ° at neutron energies of 2.5 meV, 3.7 meV and 5 meV, respectively. At 5 meV, we also use a PG crystal, which yields a scattering angle of 74.6 °. The synthetic mica and PG crystals are a great resource for accessing all final energies on MACS for  $^3\text{He}$  polarization and flipping ratio measurements. In addition, since the intensities on the Bragg peaks from mica and PG are much stronger than that from the sapphire powder sample, we can significantly reduce the incident beam flux with a strong attenuator. This allows for significantly reducing the radiation level near the sample, but still optimizing the  $^3\text{He}$  polarization and flipping ratio measurements.

In order to map the angular dependence of the opacity for a typical wide-angle cell within the full scattering angle range on MACS, we use a plastic sample so the scattered neutrons uniformly illuminate the cell. We discuss the angular dependent opacity of the wide angle cells in Sec. 5.

### 4. Reduction of magnetic field gradients on MACS

One of the main goals for experiments on MACS is to address scientific applications at high magnetic fields. More than 50 % of user experiments may utilize superconducting magnets with fields up to 11 T. Due to heavy usage of the superconducting magnet, MACS has been designed to be as non-magnetic as possible within a radius of 135 cm near the sample. Although all of the structure materials were carefully chosen when the instrument was built, some small parts near the sample area are not truly non-magnetic. These small parts are magnetized after use of the superconducting magnet. In addition, structure elements below the sample region are not non-magnetic. Although the biological shielding is mostly fabricated from non-magnetic stainless steel, we found that two locations inside the biological shielding on both sides of the neutron beam presented some field gradients. These two locations are symmetric relative to the main beam. All of these components become magnetized after use of the superconducting magnet, leading to field gradients. We found that these field gradients have significantly reduced the relaxation times of the polarizer and two analyzers.

The magnetic field gradient ( $|\vec{\nabla}B_{\perp}/B|$ ) induced  $^3\text{He}$  polarization relaxation rate is proportional to the square of the gradient and inversely proportional to the partial  $^3\text{He}$  pressure[22]. On the beam line, the space is often limited for implementation of  $^3\text{He}$  NSFs. However it is still desirable to have a field gradient of  $5 \times 10^{-4} \text{ cm}^{-1}$  or better so that the field gradient contribution to the relaxation time of the  $^3\text{He}$  polarization is 600 h or longer at a  $^3\text{He}$  pressure of 1 bar. We note that the larger field gradients can be tolerated for an in-situ  $^3\text{He}$  SEOP polarizer or analyzer.

We have established three diagnostic tools to evaluate the field gradients near the polarizer or the analyzer on MACS: (1) mapping the field directly, (2) determining the gradients from the relaxation time  $T_1$ [23], (3) determining the gradient from the NMR frequency difference among the polarizer and analyzers. Using a fluxgate magnetometer with a measurement sensitivity of  $10^{-6} \text{ mT}$ , we mapped the residual fields along three orthogonal  $X$ ,  $Y$ ,  $Z$  directions. Here  $X$  denotes along the neutron beam direction;  $Y$  denotes the direction perpendicular to the beam in the scattering plane,  $Z$  denotes the direction normal to the scattering plane.  $T_1$  is a signature of the volume averaged gradient in a  $^3\text{He}$  cell. The frequency difference provides information about the gradient between two cell locations.

After use of the superconducting magnet, the residual field was between 0.3 mT and 0.5 mT mainly in the  $Z$  direction, while the residual field in the scattering plane was negligible. The relaxation times were about 25 h and 110 h for the polarizer cell Mourvedre and the analyzer cell Giant at a holding field of 3 mT. Given that we obtained  $T_1$ 's of 330 h for the polarizer Mourvedre and 400 h for the analyzer Giant in a homogenous field with a gradient better than  $2 \times 10^{-4} \text{ cm}^{-1}$ , this indicated a field gradient of  $2.5 \times 10^{-3} \text{ cm}^{-1}$  for the polarizer cell Mourvedre and  $1.1 \times 10^{-3} \text{ cm}^{-1}$  for the analyzer cell Giant after use of the magnet. The difference in FID NMR frequency between the polarizer and one of the analyzers was about 2.3 kHz out of 99 kHz (about 3 mT), which yielded a field gradient of  $1.2 \times 10^{-3} \text{ cm}^{-1}$  for a distance of 20 cm between the polarizer and analyzer pickup coils. Therefore the resulting field gradients for the polarizer and analyzer after use of the superconducting magnet are consistent among the direct field measurement,  $T_1$  data and the difference in FID frequency. The field gradient at the analyzer was better than that at the polarizer. This is mainly due to the presence of weakly magnetized pre-sample optics and strongly magnetized magnetic cables used for controlling the beam size slit.

The short relaxation times after use of the magnet made it difficult to perform a polarized user experiment on MACS. Hence we found an appropriate demagnetization procedure to improve the relaxation times of the cells in the MACS solenoid. We started with the same maximum field applied during the magnet operation but in a reversed direction, then gradually decreased the applied field and switched the direction between two consecutive fields. This method reliably decreased the field gradient near the  $^3\text{He}$  cells. It was also important to scan the entire MACS energy range at each applied field to ensure that demagnetization occurred at each possible cell location. We found a possible field gradient dependence on cell location if demagnetization was done at one incident energy. So the relaxation times might be different at different incident energies, which would complicate time-dependent polarization efficiency corrections. An example of the demagnetization sequence after running the magnet at 9 T is (-9 T  $\rightarrow$  8 T  $\rightarrow$  -7 T  $\rightarrow$  6 T  $\rightarrow$  -5 T  $\rightarrow$  4 T  $\rightarrow$  -3 T  $\rightarrow$  2 T  $\rightarrow$  -1 T  $\rightarrow$  0.5 T  $\rightarrow$  -0.2 T  $\rightarrow$  0.1 T  $\rightarrow$  -0.05 T  $\rightarrow$  0.02 T  $\rightarrow$  -0.01 T  $\rightarrow$  0 T). It typically takes about 3 hours to perform a complete demagnetization procedure. After an adequate demagnetization procedure, there are three notable features of the residual field and more importantly the gradient: (1) the field is lower than 0.07 mT, mainly along the  $Z$  direction. The  $X$  and  $Y$  components in the scattering plane are negligible; (2) the fields at two locations near the biological shielding as mentioned earlier are significantly smaller than those measured before demagnetization; (3) the fields from the magnetized actuator cables near the polarizer are substantially lower than those measured before demagnetization. Consequently

the relaxation times of the cells are significantly improved as shown in Fig. 1a. The relaxation times of the polarizer cell Mourvedre and the analyzer cell Giant are up to 257 h and 350 h, respectively, at a holding field of 3 mT. This implies a field gradient of  $3.7 \times 10^{-4} \text{ cm}^{-1}$  and  $3 \times 10^{-4} \text{ cm}^{-1}$  for the cells Mourvedre and Giant, respectively. These indicated improvement in field gradients by a factor of 6.7 and 3.7 for the polarizer and analyzer. The shorter relaxation time of the analyzer cell Reliance compared to the analyzer cell Giant was due to a shorter relaxation time even in a very homogenous field. Most importantly, the relaxation times for the polarizer and two analyzer cells did not change between 3.7 meV and 14 meV, although they changed slightly between 2.5 meV and 3.7 meV. This allows us to perform polarized inelastic experiments for nearly the entire energy range of the MACS instrument. Furthermore the improvement in gradient was confirmed by checking the FID NMR frequency difference, which is shown in Fig. 1b. The frequency difference between the polarizer and analyzer is significantly reduced from 2.3 kHz to less than 0.4 kHz at 2.5 meV and even less than 0.2 kHz between 3.7 meV and 14 meV, which corresponds to field gradients of  $2 \times 10^{-4} \text{ cm}^{-1}$  and  $1 \times 10^{-4} \text{ cm}^{-1}$ . Since the relaxation times for the polarizer and analyzer cells we measured on MACS were close to the intrinsic ones that were measured in a homogenous field with a gradient better than  $2 \times 10^{-4} \text{ cm}^{-1}$ , we do not plan to replace the weakly magnetic parts.

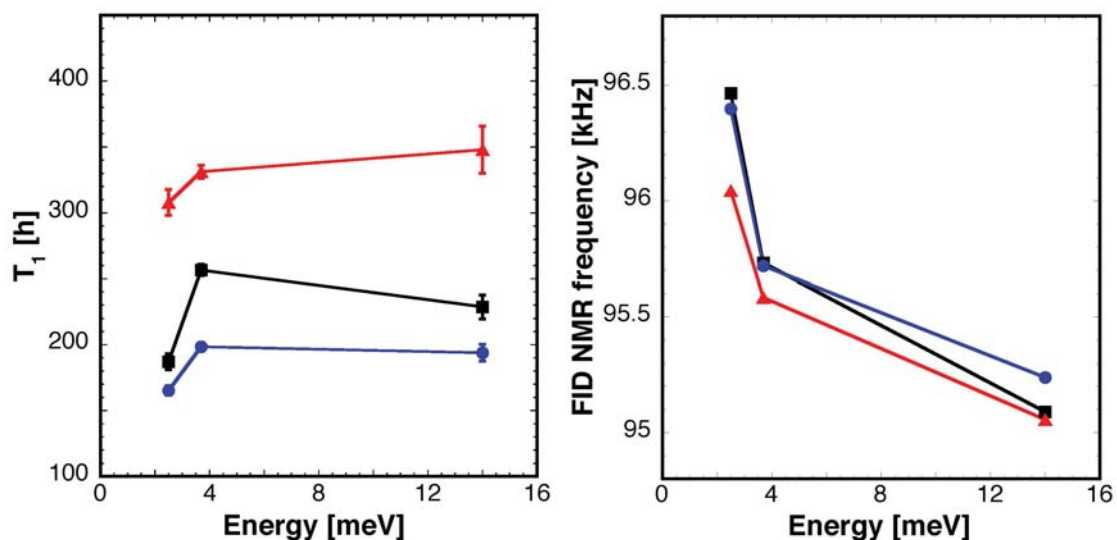


**Figure 1.** (Color online) (a) Measured relaxation times of the polarizer cell Mourvedre (solid box), the analyzer cell Giant (solid triangle) and Reliance (solid circle) at different scattered energies. (b) Fit FID NMR frequency of the polarizer cell Mourvedre (solid box), the analyzer cell Giant (solid triangle) and Reliance (solid circle) at different scattered energies. The uncertainty of the fit FID frequencies are much smaller than the size of the figure marker. All measurements were performed after performing a complete demagnetization on MACS. The demagnetization procedure is described in the text. For both measurements, the cell Mourvedre was used as polarizer and cells Giant and Reliance were used for analyzers at the positive and negative scattering angle sides, respectively. The solid lines are to guide the eye.

## 5. Wide-angle cell development

Wide-angle cell fabrication has been one of the most challenging and key elements in wide-angle polarization analysis using  $^3\text{He}$  spin filters. Substantial progress has already been made



for MEOP-based, valved, wide-angle quartz cells[9], but quartz has proved to be unsuitable for SEOP due to temperature-dependent relaxation[11, 17]. During the last decade, we have had great success in achieving long relaxation times and high  $^3\text{He}$  polarizations using sealed SEOP cells [17, 25]. These cells have mainly been fabricated from boron-free aluminosilicate glass GE180[16] due to the low  $^3\text{He}$  permeability, good alkali resistance, and great reliability to achieve long  $^3\text{He}$  polarization relaxation times.

### 5.1. Three-sectioned cell development

We have successfully made sealed, two or three-sectioned, reblown GE180 cells[11]. Fig. 2 shows an example of a sealed, three-sectioned GE180 cell named Reliance. These three-sectioned GE180 cells employed Rb-K mixtures instead of pure Rb to improve the optical pumping efficiency[26, 27]. These cells showed relaxation times up to 400 h with achievable polarization up to 80 % for the cell volume up to  $1290\text{ cm}^3$ . Using one of the NCNR SEOP systems equipped with three 100 W laser diode bars, we were able to polarize the  $1290\text{ cm}^3$  cell to 80 % with a time constant of 9 hours for optical pumping. Similar to the flat window cells in Ref. [17], it was not as reliable to obtain long relaxation times in these three-sectioned GE180 cells as compared to fully reblown GE180 cells, however the improvement did present a significant step toward success of wide angle polarization analysis using the SEOP method.

The beam size at the sample is tunable and up to 2 cm wide by 4 cm tall[13]. The beam sizes at both the polarizer and analyzer locations are calculated from the beam size at the sample, the distance from the sample, and divergences for both incident and scattered beams. When the polarizer and analyzer  $^3\text{He}$  cells were designed, all cells that are used for routine user experiments were ensured to accept the maximum beam size at each corresponding configuration[10, 11]. The maximum beam height is expected to be less than 6 cm and 5.5 cm for the three-sectioned and horseshoe-shaped cells (see Sec. 5.2), respectively. The three-sectioned cells typically have a diameter slightly larger than 8 cm, and the horseshoe-shaped cell Mozart has a height of 7.3 cm, which are large enough to cover the full beam height. A cross-sectional view of both three-sectioned and horseshoe-shaped cells is also shown in Fig. 2. The cross section is circular for the three-sectioned cell and rectangular for the horseshoe-shaped cell.

One drawback to the use of these cells as analyzers for wide angle polarization analysis is the angular dependence of the path length along the scattered beam direction. To measure the scattering angle dependence of the opacity of the analyzer cell, a plastic sample (as mentioned in Sec. 3) was used to uniformly scatter neutrons through two analyzer cells situated in experiment conditions. The opacity is a characteristic parameter of a  $^3\text{He}$  NSF, and is linearly proportional to the  $^3\text{He}$  gas density, the wavelength, and the length of the cell. The measurement was done at 3.7 meV. After correcting the detector efficiency, a map of the scattering angle dependent opacity is shown in Fig. 3. The cell Beethoven was placed on the negative scattering angle side and Reliance was placed on the positive side. Since both cells have the same geometry and similar dimensions, their angle dependent opacity showed an anti-symmetric trend, as expected. The shape of the angular dependent opacity is expected and can be modeled from the geometric shape of three-sectioned cylinders. The opacity differences between the lowest and highest values for their usable angular range are 6.2 % and 8.9 % for Reliance and Beethoven, respectively. The resulting transmission differences for an unpolarized beam would be 5.3 % and 6.9 % at a  $^3\text{He}$  polarization of 75 % for Reliance and Beethoven, respectively. The resulting neutron polarization differences would be less than 1 % for both cells. The angle dependent opacity, transmission and neutron polarization can be corrected when performing the polarization efficiency correction although this presents additional complexity due to a multi-detector bank configuration on MACS.

### 5.2. Horseshoe-shaped cell development

With three-sectioned GE180 cells we have begun polarized beam experiments on MACS, but have not yet reached a routine capability. We have also continued to develop more suitable wide angle cells. Recently, Salhi and Babcock at the JCNS developed a very large donut-shaped cell with an outside diameter of 22 cm[28]. Very recently, we have developed a method to produce a horseshoe-shaped cell by pinching off a section from a donut-shaped cell. The donut-shaped cell is produced using the similar procedure as described in the Ref. [28]. The first such cell named Mozart is shown in Fig. 2. The cell Mozart has an outside diameter of 23 cm and inner diameter of 9.2 cm with an overall volume of 1675 cm<sup>3</sup>, covering an angular range of at least 250 °. The inner diameter accommodates a 7.6 cm outside diameter cryostat tail piece. A horseshoe-shaped cell has four advantages over a three-sectioned cell: 1) since the cell is made from fully blown glass, long relaxation times can be obtained with greater reliability, 2) the circular shape yields a uniform gas path length for all scattering angles, 3) the cross section of the cell is close to rectangular, yielding a more uniform gas path length compared to a round cross section, and 4) only one <sup>3</sup>He spin analyzer is necessary, reducing the demand on our optical pumping system and FID NMR monitoring and simplifying polarization corrections from <sup>3</sup>He polarization time-dependence.

Before the cell Mozart was filled with gases of <sup>3</sup>He and nitrogen and alkali-metals, the transmission measurement was carried out to determine the variation of glass thickness with scattering angle. The measurements were done at both 2.5 meV and 5 meV using a plastic sample with and without the cell Mozart on the cold triple axis spectrometer SPINS at the NCNR. The result is shown in Fig. 4. At 2.5 meV, the glass transmission is constant for the scattering angle range between 20 ° and 120 °. At 5 meV, the transmission is nearly independent of the scattering angle. This indicated the glass thickness is uniform for the entire scattering angular range, an important result given that the cell is fully reblown and the cell fabrication process is complicated. In the future, we plan to measure this transmission on MACS. We filled the cell Mozart to 1.07 bar <sup>3</sup>He gas and distilled an appropriate ratio of rubidium and potassium metals[17]. We were successful in obtaining a relaxation time of 350 h in the first attempt. The K/Rb vapor mixture ratio at an operating temperature of 215 °C was measured to be 5, optimized for optical pumping efficiency and <sup>3</sup>He polarization. For comparison, a map of the opacity for the cell Mozart as a function of the scattering angle is also shown in Fig. 3. The cell Mozart is optimized at 3.7 meV. Unlike both cells Reliance and Beethoven, the cell Mozart showed a scattering-angle independent opacity on both sides of the main beam. The opacity is slightly lower at positive angles for the cell Mozart than that at negative ones, which is due to imperfect coincidence of the centers of the inner hole and the outer circle when forming a donut-shaped cell. More horseshoe cells will be made in the future for a routine capability of wide angle polarization analysis on MACS. The cell Mozart was recently polarized using one of the NCNR SEOP systems[2] equipped with three 100 W laser diode bars. We obtained a <sup>3</sup>He polarization of 78 % based on a neutron transmission measurement.

The opacity can change with the beam height as this has been modelled for other instrument geometries[30]. For polarized MACS experiments we have done so far, we have measured opacities for each cell to accommodate a different sample size. A typical sample height was about 2.5 cm. We took particular care to ensure a three-sectioned analyzer cell being reliably located on the beam line in the same way for every experiment. To accomplish this, we designed an aluminum structure (referred to as the thimble[10]) to (1) support the cryostat and (2) to isolate the analyzer cells from the cryostat so that the <sup>3</sup>He glass cells are protected. Since there is only a few millimeter gap between the thimble and the analyzer cells due to space constraint, aligning the analyzer cells is straightforward by placing the cells close to the thimble simulator with an additional alignment tool between the two cell ends on either side of the main beam.



**Figure 2.** (Color online) Three-sectioned wide-angle cell as developed[11] (left photo). Each cell covers a scattering angle range between  $90^\circ$  and  $110^\circ$ ; An example of the recently developed horseshoe shaped wide angle cells (right photo). A cross-sectional view of both cells is shown in the middle of the photo. A circular cross section indicates the three-sectioned cell and a rectangular cross section indicates the horseshoe-shaped cell. A single horseshoe cell covers scattering angle of up to  $260^\circ$ . The cell Mozart has an outside diameter of 23 cm, an inner diameter of 9.2 cm and a height of 7.5 cm.

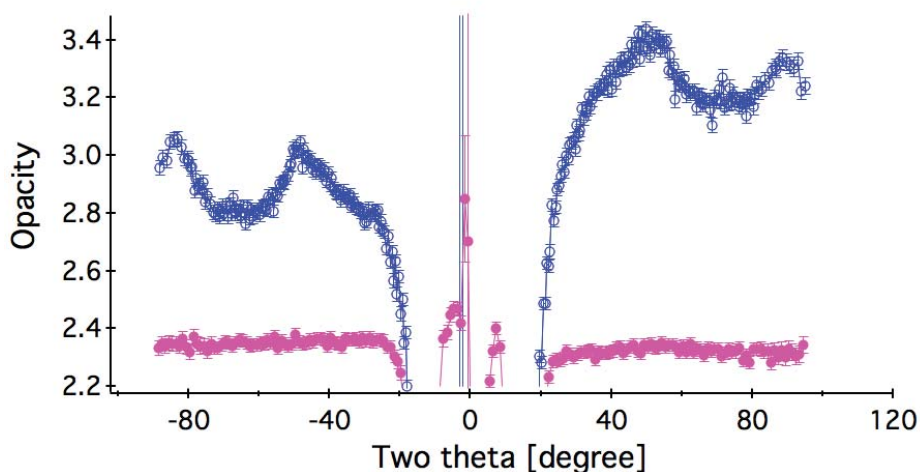


**Figure 3.** (Color online) Measured opacity as a function of the scattering angle for the three-sectioned cells (open circles) and the horseshoe cell (solid circles). The opacity of a  $^3\text{He}$  cell is linearly proportional to the  $^3\text{He}$  gas density, the wavelength, and the length of the cell. The measurements were done at 3.7 meV on MACS. For three-sectioned cell measurements, the cell Beethoven was located on the negative scattering angle side and the cell Reliance was located on the positive scattering angle side.



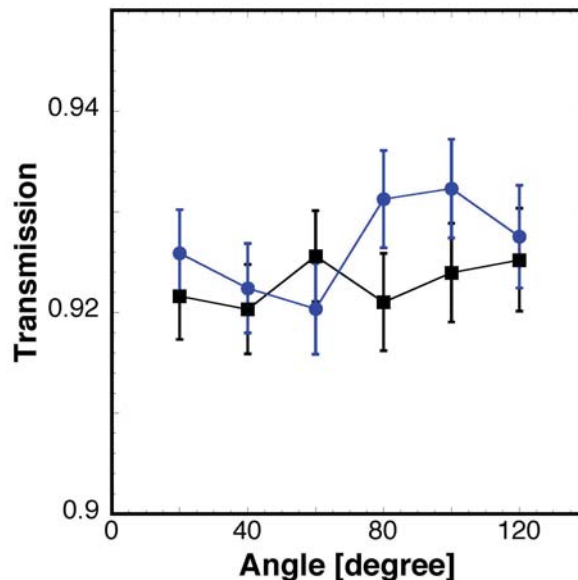


**Figure 4.** (Color online) Measured glass transmission of the unfilled Mozart at different scattering angles at energies of 2.5 meV (solid box) and 5 meV (solid circle). The measurements were done on the cold triple axis spectrometer SPINS at the NCNR. Nearly scattering-independent transmission implies that the glass thickness is uniform for the entire scattering angle range. Given that the cell is fully reblown, it is remarkable. The solid lines are to guide the eye.

## 6. Conclusions

We have established a new procedure for the  $^3\text{He}$  spin filter characterization using different standard samples, either synthetic mica or PG crystals depending on the energy. This allows for more efficient and convenient measurements of transmission and flipping ratio measurements. We have found an appropriate demagnetization procedure to significantly reduce the residual field gradient present on MACS, which allows us to reliably achieve relaxation times of 200 h or higher for the polarizer and 300 h or higher for the analyzer. Most importantly, these relaxation times are independent of the incident energy, a characteristic feature necessary for polarization analysis of inelastic scattering. We have developed horseshoe shaped cells that present advantages over three-sectioned wide angle cells in achieving longer relaxation times with greater reliability, scattering-angle independent cell opacity, and more efficient operation in polarized beam preparation and polarization efficiency correction. We obtained a relaxation time of 350 h and achieved  $^3\text{He}$  polarization of 78 % for the first filled horseshoe cell. With this substantial progress, we will soon have routine capability in wide angle polarization analysis on MACS.

## Acknowledgments

We thank Jeff Anderson and Jack Fuller of the NIST glassblowing and optical shops. In addition we thank J.W. Lynn and C.F. Majkrzak for their help in loaning synthetic mica crystals and a PG crystal. We acknowledge Leland Harriger for his help in the glass transmission measurement on SPINS. The development and application of neutron spin filters was supported in part by the U.S. Dept. of Energy, Basic Energy Sciences. The work utilized facilities supported in part by the National Science Foundation under Agreement No. DMR-1508249.

## References

- [1] Abragam A 1961 *The Principles of Nuclear Magnetism* Oxford University Press, Oxford, England
- [2] Chen WC *et al.* 2014 *Journal of Physics: Conference Series* **528** 012014
- [3] Andersen KH *et al.* 2005 *Physica B* **356** 103
- [4] Babcock E, Ioffe, A 2011 *Journal of Physics: Conference Series* **294** 012005
- [5] Jiang CY *et al.* 2013 *Physics Procedia* **42** 191
- [6] Beecham CJ *et al.* 2011 *Physica B* **406** 2429
- [7] Kira H *et al.* 2011 *Journal of Physics: Conference Series* **294** 012014
- [8] Heil W *et al.* 2002 *Nucl. Instrum. Meth. A* **485** 551
- [9] Andersen KH *et al.* 2009 *Physica B* **404** 2652
- [10] Fu CB *et al.* 2011 *Physica B* **406** 2419
- [11] Ye Q *et al.* 2013 *Physics Procedia* **42** 206
- [12] Babcock E *et al.* 2014 *Journal of Physics: Conference Series* **528** 012018
- [13] Rodriguez-Rivera A *et al.* 2008 *Meas. Sci. Technol.* **19**, 034023
- [14] <http://www.ill.eu/instruments-support/instruments-groups/instruments/d7/description>
- [15] <http://www.mlz-garching.de/dns>
- [16] GE Lighting Component Sales, Bldg. 315D, 1975 Noble Rd., Cleveland, OH 44117. The largest standard GE180 tubing diameter is 16 mm; the 25 mm tubing was procured through a special glass run. Certain trade names and company products are mentioned in the text or identified in an illustration in order to adequately specify the experimental procedure and equipment used. In no case does such identification imply recommendation or endorsement by the National Institute of Standards and Technology, nor does it imply that the products are necessarily the best available for the purpose.
- [17] Chen WC *et al.* 2011 *Journal of Physics: Conference Series* **294** 012003, and references therein
- [18] Thampy V *et al.* 2012 *Phys. Rev. Lett.* **108**, 107002
- [19] Jones GL *et al.* 2000 *Nucl. Instrum. Meth. A* **440** 772
- [20] McCauley JW, Newnham RE, and Gibbs GV 1973 *American Mineralogist* **58** 249
- [21] Boeuf A *et al.* 1983 *Synthetic Metals* **8** 307
- [22] Cates GD, Schaefer SR and Happer W 1988 *Phys. Rev. A* **37** 2877
- [23] McIver JW, Erwin R, Chen WC and Gentile TR 2009 *Rev. Sci. Instrum.* **80** 063905.
- [24] Babcock E *et al.* 2006 *Phys. Rev. Lett.* **96** 083003
- [25] Chen WC *et al.* 2014 *J. Appl. Phys.* **116** 014903
- [26] Babcock E *et al.* 2003 *Phys. Rev. Lett.* **91** 123003
- [27] Chen WC, Gentile TR, Walker TG, and Babcock E 2007 *Phys. Rev. A* **75** 013416
- [28] Salhi Z, Babcock E, Pistel, P, and Ioffe A 2014 *Journal of Physics: Conference Series* **528** 012015
- [29] Goland AN, Sondericker Jr. JH and Antal JJ 1959 *Rev. Sci. Instrum.* **30** 269.
- [30] Chen WC, Erwin R, and Watson SM, 2013 *Physics Procedia* **42** 163-170.